An Automated Fabrication Strategy to create Patterned Tubular Architectures at Cell and Tissue scales

Rebeen Othman*[1], Gavin Morris*[1], Disheet A Shah[1], Stephen Hall[2], Graham Hall[3], Keith Wells[4] and Kevin M. Shakesheff[ψ1], James E. Dixon*[1]

[1]School of Pharmacy, Wolfson Centre for Stem Cells, Tissue Engineering, and Modelling (STEM), Centre of Biomolecular Sciences, [2]Medical Engineering Unit, School of Medicine; University of Nottingham, Nottingham, NG7 2RD, UK; University of Nottingham, Nottingham, NG7 2RD, UK. [3]Tannlin Ltd., Newmoor Industrial Estate, Irvine, KA1 2DJ, UK. [4]Trent Thermal Technology, Nottingham Science Park, Nottingham, NG7 2QP, UK.

*Co-first authors

ψCorrespondence should be addressed to:

Kevin M. Shakesheff

kevin.shakesheff@nottingham.ac.uk

Wolfson Centre for Stem Cells, Tissue Engineering, and Modelling (STEM)

Centre for Biomolecular Sciences

University of Nottingham

University Park

Nottingham NG7 2RD, UK

Tel: +44 (0) 115 82 32003

Fax: +44 (0) 115 84 68002

Short Running Title: *In vitro* automated fabrication of living tubular architectures

The use of materials to impose tissue-like architecture at cell resolution will be important if engineered functional replacements for damaged cardiovascular, pulmonary, renal or digestive tissues are to be authentically engineered. Here, we demonstrate a coordinated system for the fabrication and subsequent culture of tubular tissues composed of multiple layers, cell-types and materials with physiological dimensions and defined architectures at cell resolution. We developed an automated tube fabricator (ATF) that rolls 2D-matrices into 3D-tubular constructs directly from cells, hydrogels and scaffold biomaterials. Coordinated use of surface modification strategies allows 2D cell sheets and cell/biomaterial composites (i.e. hydrogels or electrospun scaffolds) to be fabricated which may be transferred into a perfusion bioreactor in a rapid and standardized procedure. To exemplify our strategy we fabricated structures resembling human mammary artery and gut; these can be imaged *in situ* and real-time electrical resistance measurements performed of the vessel walls, allowing non-invasive assessment of viability and functionality. Our system allows patterning at cellular resolution with variable tissue thickness, length, luminal diameter, and constituent biomaterial. This inherent flexibility will allow the recapitulation of the complex hierarchical biological architectures and generate functionality found natively *in vivo*.

Introduction

Various obstacles hinder tissue engineered vessel development including recreating the substantial mechanical strength and biological activity *in situ* grafts require on transplant. Furthermore these conduits need to be immunologically inert and non-thrombotic for successful long-term post-transplantation patency and for clinical adoption (Kakisis et al., 2005, Baguneid et al., 2006). Fundamental construct fabrication considerations include; dimension standardization, and for biologically active architectures, factors such as seeding, positioning and patterning of cells within different layers throughout tissues. To address these, various methodologies have been applied including synthetic scaffolds, biocompatible natural scaffolds, cell sheet technologies, automated (McAllister et al. 2006) or self-assembly of vessels (Baguneid et al., 2006, Kakisis et al., 2005, Peck et al., 2012, Nerem and Seliktar, 2001, Kubo et al., 2007, Williams et al., 2009). Some models have shown good patency in animal models (Niklason et al., 1999, Kim et al., 2008, Shum-Tim et al., 1999, Wang et al., 2013), with few progressing to human trials (Shin'oka et al.,

2005, Shin'oka et al., 2001, McAllister et al., 2009). This limited success highlights the necessity to improve graft fabrication processes and facilitate the use of multi-phase materials to create tissues (Peck et al., 2012, Baguneid et al., 2006). Multilayer tubes have been engineered using various approaches including manually rolling cell sheets around a mandrel (L'Heureux et al., 2006, L'Heureux et al., 1998, Seliktar et al., 2000), tubular constructs requiring external structural supports to prevent tube disassembly (Papenburg et al., 2009), cell sheet rolling technologies (Kubo et al., 2007), or self-rolling stretched synthetic materials (Yuan et al., 2012). Manual rolling with or without additional external support is technically complex and requires lengthy tissue maturation, whilst the presence of stabilizing materials prevents usefulness in downstream applications. Self-rolling materials are generally not biocompatible for long-term viability, and the mechanical forces placed on cells may directly affect cell behaviour (Engler et al., 2006). The application of cell sheet patterning technologies allows precise positioning of cells within a 2D layer (Williams et al., 2009), however the only previous example of an automated tube fabrication strategy required sheets to be suspended in solution, preventing controllable sheet orientation (Kubo et al., 2007). Here, we focused on devising a methodology to fabricate example tissues with these attributes.

Material and Methods

Materials

Materials were purchased from Sigma-Aldrich (Dorset, UK) unless stated otherwise. NIH-3t3 mouse embryonic fibroblasts (3T3s), human umbilical vein endothelial cells (HUVECs), BJ6 fibroblast cells and CACO-2 cells were obtained from the LGC Standards (Middlesex, UK). Primary human airway smooth muscle cells (SMCs) were isolated from bronchial biopsies at the Glenfield Hospital (Leicester, UK) as described previously.(Kaur et al., 2006) The research was approved by the Leicestershire Ethics Committee, and patients gave their written informed consent. HUVEC media was supplied by Promocell (Heidelberg, Germany). DMEM media, rat tail collagen I, mouse monoclonal anti-E-cadherin, and rhodamine-conjugated secondary antibody were obtained from Invitrogen Life Technologies (Paisley, UK). Lentiviral labelling of cell lines was performed as described previously (Dixon et al. 2011, Paik et al. 2012). Cells were infected with enhanced green fluorescent protein (GFP)- or monomeric red fluorescent protein (mRFP)-labelled lentivirus at confluence and selected with puromycin for 7 days which produced >95% labelled cells confirmed by flow cytometry.

Cell Maintenance

Cells were cultured in isolation at 37°C in a 5% CO_2 incubator. 3T3, SMC, CACO-2, and BJ6 cells were maintained in DMEM media containing 10% (*v/v*) FCS and 1% penicillin/streptomycin. HUVEC cells were maintained in endothelial cell growth media supplemented with 0.02% (v/v) FCS, 0.004% (v/v) endothelial cell growth supplement, 0.1ng/ml epidermal growth factor, 1ng/ml basic fibroblast growth factor, 90 µg/ml heparin, 4 µg/ml hydrocortisone, and 1% penicillin/streptomycin.

Preparation of Collagen cell sheets

Collagen sheets (2mg/ml; 25x15mm^2) loaded with cells (3t3s, 2x10^6/sheet) were crosslinked within filter paper frames for 1hr at 37°C and were cultured until confluency (3 days). Filter paper frames were used to transfer sheets to the ATF and the frame excised before fabrication.

Preparation of Thermo-responsive Surfaces and Monolayer or Micro-patterned Cell Sheets

Non-treated tissue culture plastic was coated with 5µl/cm^2 of 5% PNIPAAm (w/v) in distilled water using an EClA500 HP-CS gravity-fed air-brush at 20 pounds per square inch (psi) (The Airbrush Company Ltd., UK). For grafting these were heated to 65°C for 12 hours. 5µl/cm^2 of 100% FCS was deposited on PNIPAAm-coated dishes by air brushing coating the full surface for monolayers or through micropatterned stencils (Tannlin Ltd, UK) for patterning cells (Paik et al., 2012). Cells (6x10^6 cells) were seeded onto surfaces or micropatterns in media without FCS or Ca^{2+}. For monolayers after confluency was achieved alginate-wetted (1.2% w/v) filter paper frames were placed onto the monolayer, the alginate crosslinked with 135mM $CaCl_2$ to adhere to the underlying outer portion of the monolayer and the sheet detached through reduction in temperature to 4°C and gentle agitation. For patterns alginate (1.2% w/v) was used to overlay the pattern within a filter paper frame, the alginate crosslinked and detached as above. Filter paper frames were used to transfer sheets to the ATF and the frame excised before fabrication.

Electrospun Scaffold Fabrication

Electrospun scaffolds was produced in a vented chemical fume hood at room temperature using 10% PET (w/v) (foods grade drinking bottle quality) dissolved in a 1:1 trifluoroacetic acid (TFA):di-chloromethane (DCM) (Fisher Chemicals, Loughborough, UK). Polymer solution was loaded into a syringe attached to a blunt 23-gauge (G) needle (BD Falcon™, Oxford, UK) and placed in a pump-driver (Harvard Apparatus Ltd., Kent, UK) extruding at 0.5ml/hr. A 15kV voltage was applied and nanofibres were collected on a steel collector plate positioned 15cm from the needle tip. Scaffolds were attached to Perspex frames and sterilized by UV-irradiation for 30min. For seeding scaffolds were soaked in media prior to CACO-2 cell seeding (1x10^6 Caco-2 cells/25x15mm^2 scaffold). Perspex frames were used to transfer sheets to the ATF and the scaffold excised before fabrication.

Fabricating Vessels

The ATF (developed and manufactured by the Medical Engineering Unit, University of Nottingham) consists of stepper-motor driven modules, a mandrel rotation module driven by two inversely rotating facing stepper-motors and a sample delivery module, and a stage to deliver the material to the mandrel rotation module. Distance between the stage and mandrel is manually (or automatically) controlled to bring the sample in contact with mandrel. Using the programmable system the automated fabrication was initiated and the mandrel rotation module rotated (0.1-1 rotations/second) to draw up the sample. This action occurs simultaneously as the stage advancing; the stage covering the same distance as the circumference of the mandrel at the same rate as mandrel rotation. The fabricated tube (directly integrated into the tube holder mounts) was transferred into the jig. For Fibrin hydrogel bonding; 20µl/cm^2 of 16mg/ml Human Fibrinogen was incubated with cell sheets, hydrogels or biomaterial for 5mins at 25˚C. 20µl/cm^2 of 200U/ml Human Thrombin was either airbrushed onto the tube mounts or incubated with the previously fabricated layer for 5mins at 25˚C. Bonding of the tube mounts and the first layer was allowed to take place for 5mins before fabrication.

Transepithelial Electrical Resistance (TEER) Measurements with Calcium Depletion

CACO-2 populated tubular constructs connected to the bioreactor system had electrodes inserted within the tube lumen and the perfusion chamber that were connected to an EVOM^2 volt-ohm-meter (World Precision Instruments, Hitchin, UK). Background conductance was removed by subtracting acellular scaffold readings. Media was replaced with CRB (Dixon et al. 2014) for 5min at room temperature which was then replaced by growth media (which contains 2mM $CaCl_2$). TEER readings were taken periodically over a 24hr time period and are expressed as a percentage of the initial TEER reading (Ω/Ω_0)/cm^2.

Dextran Permeability

CACO-2 populated tubular constructs were incubated in serum-free media at 37°C for 1hr. A solution containing both 4kDa FITC-tagged dextran and 70kDa-Rhodamine-tagged dextran (1mg/ml) was added to the tube lumen. Media in the perfusion chamber was replaced with CRB for 5min at room temperature

before replacing with normal media. Samples were collected from the perfusion chamber over a 2hr period post-CRB application and fluorescence quantified on a plate reader (excitation 520nm/emission 590nm) (Tecan Infinite M200, Reading UK).

Immunocytochemistry

Samples were calcium depleted for 5min before immediate fixation and permeabilization using 100% methanol at -20^{o}C. Non-specific antibody binding was reduced by incubation in 3% (w/v) bovine serum albumin solution. Samples were incubated with anti-E-cadherin antibody overnight at 4^{o}C, with protein expression visualised with species-appropriate secondary antibody.

Construct Visualization

Composite tubular formations were visualized using a Nikon Eclipse TS100 Microscope (Nikon Instruments, Surrey, UK). Entire surface micropatterns images were captured by Nikon SMZ 1500 microscope with a SPOT insight camera. To view 3D tubes, and E-cadherin staining a TCS LSI super zoom confocal microscope was used (Leica Microsystems, Milton Keynes, UK).

Data and Statistical Analysis

Data are presented for cells cultured on at least three separate occasions and are expressed as mean±SEM. Data were analysed (GraphPad Prism, San Diego CA) using unpaired T-test.

Results

Development of the ATF

To produce viable, multi-layered, 3D-tubular architectures from 2D-cellular sheets, we developed the ATF to perform pre-determined automated tube rolling protocols (Figure 1A & B). We have developed this technology to be unrestricted as to the material used for fabrication and to allow patterned materials to be employed in an orientated fashion. The device is integrated into a sterile culture hood and consists of 3 stepper-motor driven modules: i) a 'mandrel rotation' module driven by two inversely rotating facing stepper-motors, ii) a 'sample delivery' module; a stage to deliver the material to the mandrel rotation module, and iii) a 'transfer module'; a system to transfer the construct to a compatible perfusion bioreactor. The fabrication process is complete within minutes and can rapidly reset to build multi-layer, multi-phase or multi-material architectures. The distance between the stage and mandrel is automatically or manually controlled to bring the 2D-material in contact with mandrel (Figure 1A, N^{o} 10). Fabrication is remotely initiated and the mandrel rotates at the same speed as the delivery stage (programmed from 0.1-1 rotations/second) to draw up and roll the sample. If required, thrombin/fibrinogen bonding can be employed to integrate multiple-phases; the mandrel coated with thrombin and the cell sheet/material treated with fibrinogen solution (Figure 1C). Contact between the thrombin (mandrel) and the fibrinogen (sheet/material) creates a fibrin hydrogel which securely bonds the surfaces. During fabrication, fibrin forms crosslinks between adjacent layers and creates a fully adhered structure. Fabricated tubes are securely integrated into tube holder mounts (Figure 1A, N^{o} 4) and transferred to sterile culture jigs using the rotating tube transfer Y-arm (Figure 1A, N^{o} 3). This can then be installed in the complementary bioreactor system (Figure 3A), ensuring no further tube manipulation is required for effective construct perfusion. (Tube fabrication demonstrated in Video S1). If necessary the fabricated vessels can be detached from the bioreactor manually which is not prevented by using Fibrin within the structure.

Fabrication of vessels with varying dimensions and phases

Construct dimensions can be manipulated by varying different parameters: Wall thickness is determined by the 2D-material thickness and/or number of rotations around the mandrel (5µm->1cm). Length can be

adjusted by repositioning the mandrel rotation motors (Figure 1B; purple arrows) and/or varying cell-sheet width (<1mm-5cm). Here we demonstrated short vessels of several centimetres but clinically relevant lengths (15-60cm long) could be fabricated by modifying the motor distance and using further cell sheets to bond the junctions between several tube sections. Luminal diameter is varied using differently sized holder mounts (100µm-5cm). This flexibility ensures constructs possess dimensions comparable to various human tubular tissues. As examples, using a PET electrospun scaffold and alginate composite, we fabricated single-phase tubular architectures with dimensions applicable to grafts from the aorta, gut, trachea, medium diameter arteries and urethra (Figure 1D).

Multi-phase constructs are fabricated by sequentially rolling cellular-sheets/materials. A tri-phasic tubular structure consisting of a single cell monolayer and two cell-seeded collagen gels was fabricated (Figure 2A) as an exemplar. Initially a GFP-labelled NIH3T3 (GFP-3t3s) cell monolayer was rolled around the mandrel (1.05 rotations, 5µm layer thickness), followed by an mRFP- (mRFP-3t3s) and a GFP-3t3s seeded collagen gel (both 1.05 rotations, ~250µm layer thickness) (Figure 2A-E). Cell monolayers were created by surface modification of non-tissue culture-treated surfaces airbrushed with the temperature-sensitive polymer poly(N-isoproplacrylamide) (PNIPAAm) and foetal calf serum (FCS) prior to cell culture to confluence (Williams et al., 2009). PNIPAAm grafting was conducted using temperature-dependent absorption (65°C for 12 hours). This was chosen over other techniques such as UV- or microwave-radiation due to ease of processing samples. For simplicity and before temperature-sensitive detatchment, cell monolayers were cross-linked to an outer paper frame coated in alginate. This suspends the monolayer between the support allowing it to be easily transferred to the ATF for fabrication (Figure S1). A temperature reduction (4°C) allows the harvest of a complete cell monolayer sheet (Figure S2A) without damaging cell-deposited extracellular matrix (ECM)(Shimizu et al., 2001, Shimizu et al., 2006). We analysed the complete fabricated tubes demonstrating layer integrity was maintained, with no significant cell migration into adjacent phases (Figure 2D: hydrogel to hydrogel; Figure 2E: monolayer to hydrogel) after 7 days of culture. Importantly however layers were integrated with cells at the phase surfaces in direct contact (Figure 2D; white arrow show integration, black arrows show phase interface).

Creation of patterned architectures

To demonstrate the utility of our technology inter- and intra-layer cell patterning (with micrometre resolution over an extended distance) within the tubular architectures was achieved by adapting our previous high-resolution cell patterning technology (Figure S2A)(Paik et al., 2012). We employed micropatterned stencils and airbrushing to generate 50µm-wide lines of PNIPAAm interspersed with 50µm intervals on non-tissue culture plastic surfaces which we used to pattern GFP-3T3s (Figure 2F). We chose such large spacing between patterned lines to help visualisation however smaller gaps could be used to create orientated sheets rather than simple micropatterns. Patterns could be transferred by overlaying and detaching alginate-crosslinked sheets. These sheets maintained cellular patterning and were fabricated into vessels using the ATF (Figure 2G). In many tubular tissues luminal capacity is controlled by the surrounding smooth muscle cells (SMCs) which orientate uni-axially to ensure co-ordinated muscle contraction (Dobrin, 1978). We therefore used this patterning to demonstrate effective cell alignment that can be directed into a helical orientation (evident in the larger airway bronchioles and small resistance arteries)(Jeffery, 2001, Rhodin, 1980) or herringbone alternating orientations (found in larger elastic arteries which maintain wall structural integrity)(Rhodin, 1980). The herringbone motif was recapitulated using micro-patterning and ATF sheet fabrication; GFP-3T3 and mRFP-3T3 micropatterned cell sheets at 60° (mRFP-3T3) and 120° (GFP-3T3) from horizontal respectively (Figure S3; example orientation). These two layers were fabricated sequentially to produce a 3D-tubular architecture with a herring bone motif found in native blood vessels (Rhodin, 1980) (Figure 2H), and previously modelled in 2D (Williams et al., 2011). Using materials such as aligned electrospun fibres would be useful to create orientation of cells which precisely mimic the *in vivo* situation (Morris et al. 2014).

Fabrication of an arterial biomimetic

We recapitulated a complete vascular conduit comprising of four cell layers to mimic the individual regions found within a blood vessel wall (Rhodin, 1980) (Figure 2I) with dimensions comparable to an adult internal mammary artery (IMA) routinely used in heart bypass surgery (2.3-3.4mm external diameter, 0.6-0.75mm

wall thickness)(van Andel et al., 2003, Karaman et al., 2012). To ensure clear visualization of each cell-type post-fabrication, GFP-labelled HUVEC endothelial cells (GFP-HUVEC), mRFP-labelled smooth muscle cells (mRFP-SMC), and GFP-labelled BJ6 fibroblast cells (GFP-BJ6) were generated by lentiviral genetic modification (Dixon et al., 2011). Initially, individual 2D-sheets of GFP-HUVEC cells ($3x10^6$ cells), two aligned sheets of mRFP-SMC ($1x10^6$ cells), and a sheet of GFP-BJ6 cells ($3x10^6$ cells) were cultured as 2D-sheets for 2 days before sequential cell-sheet rolling and tube imaging (Figure 2J). The two SMC layers were rolled in the same orientation to allow visualization of the individual cell layers.

Creation of tubular tissues with Gut-like Barrier function

Electrospun scaffolds are another biomaterial extensively used in tissue engineering that can mimic the 3D nano-topography of basement membranes on which epithelial cells reside in tubular architectures (Dalton et al., 2012, Teo and Ramakrishna, 2006, Booth et al., 2012). Exploitation of such technology has been mainly concentrated on regenerative purposes, with tissue engineered vascular (Shin'oka et al., 2005, Patterson et al., 2012, Kim et al., 2008, Wang et al., 2013) and tracheal (Jungebluth et al., 2011) grafts successfully transplanted into humans. To demonstrate the versatility of the ATF in fabricating various biomaterials, a simple epithelial tubular structure populated with the gut epithelial CACO-2 cell-line on a nanofibrous polyethylene terephthalate (PET) electrospun scaffold was created (Figure 3C). The epithelium's primary function is to provide a physical barrier between adjacent environments whilst allowing a controlled para-cellular flow of nutrients and ions, and maintaining cellular polarization and structural integrity (Mullin et al., 2005). Inter-cellular barrier junctions consist of tight- and adheren-junctions to control barrier integrity and porosity (Schneeberger and Lynch, 2004, Gumbiner, 1996). The trans-epithelial electrical resistance (TEER) was measured as an indicator of barrier function. During initial 2D-cell sheet culture period, CACO-2 cells showed a TEER increase, with negligible increases seen after 10 days indicating functional barrier formation. 3D-tubular, cell-populated scaffolds were fabricated on the ATF and transferred to the compatible bioreactor system (Figure 3A). Real-time TEER measurements within the bioreactor system were taken by inserting electrodes inside the lumen of the tube (Figure 3A [V2 & I2] & 3B), and externally to the construct in the bioreactor perfusion chamber (Figure 3B, V1 & I1). These

electrodes were connected to an EVOM^2 machine measuring voltage (V1 & V2) and amplitude (I1 & I2) to quantify resistance across the tubular wall (Figure 3A).

Relative levels of extracellular and intracellular calcium can directly affect epithelial layer barrier integrity (Cereijido et al., 1978, Gumbiner and Simons, 1986), a phenomenon applied to examining the modulation of barrier integrity in gut and kidney models (Gumbiner and Simons, 1986, Ye et al., 1999, Ivanov et al., 2004b, Kwak et al., 2012). This short-term, reversible effect is induced through the dis-assembly of the inter-cellular junctional complexes (Ivanov et al., 2004a). CACO-2 populated tubes were incubated in a calcium reducing buffer (CRB), known to chelate calcium (Dixon et al. 2014) for 5 minutes before replacing with normal media (containing 2mM Ca^{2+}) for a further 24hrs. Epithelial barrier permeability during this period was measured through TEER and para-cellular permeability. The reduction of extracellular calcium produced an instantaneous drop in TEER (67±5vs 144±8 Ω/cm^2; mean ± SEM, n=3) with the re-introduction of calcium providing an equally robust restoration in electrical resistance that returned to initial levels after 24hrs (Figure 3E). Inter-cellular junction integrity was visualised by immunostaining the adheren-junction protein E-cadherin at 5min and 24hrs post-calcium depletion. The classic “chicken-wire” E-cadherin distribution prior to calcium reduction was disrupted at 5min and restored after 24hrs (Figure 3D). In parallel, barrier integrity was monitored by small-molecule permeability. Using fluorescently-labelled dextran (4kDa FITC-dextran and 70kDa Rhodamine-dextran) allowed the analysis of different sized molecule diffusion within individual samples. Dextran was applied to the lumen of either blank electrospun scaffold tube, or a CACO-2 populated tube, and samples were taken from the perfusion chamber over a 2hr time course. Diffusion through acellular tubes was greater than cellular tubes (Figure 3F), whilst CRB treatment of cellular tubes significantly increased the rate of dextran diffusion over the time course. Lower weight dextran (4kDa) showed an increased diffusion rate compared to larger dextran molecules (70kDa) (Figure 3G). These data indicate CACO-2 fabricated architectures possess functional barrier properties that restrict para-cellular diffusion in a size dependent manner. Therefore we fabricated an intestinal tubular tissue that could be employed for drug screening strategies.

Discussion

Here we have demonstrated an automated fabrication system to create multi-layer, multi-phasic, patterned tubular structures in which biomaterials, hydrogels or cells can be used as the base material. In conjunction with previously described patterning technology (Paik et al. 2012) and temperature-responsive polymers (PNIPAAM) (Williams et al., 2009) this technology allows precise positioning of cells in 3D architectures.

This study has demonstrated that dimension standardization can be achieved in biologically active architectures and issues such as seeding, positioning and patterning of cells within different layers throughout tissues can be addressed directly during fabrication beyond the attempts of other studies (Peck et al., 2012, Baguneid et al., 2006). Manual fabrication of vessels used in previous studies (L'Heureux et al., 2006, L'Heureux et al., 1998, Seliktar et al., 2000) is not easily achievable when multi-layer, –phasic patterned architectures are required which prompted the development of the ATF system. An automated system presents theoretical advantages over manual fabrication. However cost and system complexity must be offset with an improvement in vessel quality, speed of production and less need for technical ability needed for manual fabrication. Previous cell sheet rolling technologies (Kubo et al., 2007; McAllister et al 2006) have produced fabricated vessels however the technicality of manipulating delicate and hydrated hydrogels or cell sheets prompted us to develop a system in which 2D materials are fed into the fabrication mechanism yielding much more reproducible constructs and allowed patterned cellular structures to be fabricated (Williams et al., 2009). Furthermore by integrating the ATF system to transfer constructs to perfusion chambers directly the inherent variability of manual manipulation to allow bioreactor mounting and perfusion is removed. We demonstrated the use of fibrin to bond sheets during fabrication. Fibrin confers the advantage of rapid adherence between fabricated sheets but does have it disadvantages; Fibrin inclusion adds cost and could interfere with fusion of layers due to the biological activity of cells following fabrication during maturation. Furthermore the fibrin component was not sufficient to provide sufficient mechanical strength to create viable blood vessel mimetic constructs. Importantly, Fibrin is not essential to our system and its use could be emitted. Further analyses regarding

any thrombogenic activity of Fibrin in these constructs will also need to be tested before *in vivo* translation however this is unlikely (Kheirabadi et al. 2006).

Even with our technology, materials that are fully bioactive and provide the substantial mechanical strength will need to be developed if living tissue is to be engineered as vascular grafts. However as the ATF system can be employed with any 2D material this methodology could be used to fabricate vessels with such materials (Kakisis et al., 2005, Baguneid et al., 2006). Using the ATF system for fabrication of vasculature employing materials with the correct mechanical properties is now the focus of future work.

Conclusion

This novel automated platform allows accurate, standardized and repeatable fabrication of tubular architectures; comprised of multiple compact, stable and secure cell and/or material layers. These fabricated tissues are directly transferred to a compatible perfusion bioreactor without further manipulation. Rolling of each layer takes less than a minute and because no external material is required to maintain the structure except the cells with or without a biomaterial, it can be considered as an authentic living structure. We demonstrated our systems utility in fabricating vessels with arterial-like cell patterning and gut-like barrier function. This technology is easily adaptable to fabricate multiple biomaterial-types to engineer a variety of biologically stable tissues directed for regenerative or *in vitro* diagnostic protocols.

Acknowledgements

This work was funded by the ERC and UKRMP. We thank Tannlin Ltd. for stencil manufacture and the University of Nottingham Medical Engineering Unit (MEU) in the design and manufacture of the ATF and accessories. We thank WPI Ltd for helpful discussions to develop real-time tube resistance measurements.

References

BAGUNEID, M. S., SEIFALIAN, A. M., SALACINSKI, H. J., MURRAY, D., HAMILTON, G. & WALKER, M. G. 2006. Tissue engineering of blood vessels. *Br J Surg,* 93**,** 282-90.

BOOTH, A. J., HADLEY, R., CORNETT, A. M., DREFFS, A. A., MATTHES, S. A., TSUI, J. L., WEISS, K., HOROWITZ, J. C., FIORE, V. F., BARKER, T. H., MOORE, B. B., MARTINEZ, F. J., NIKLASON, L. E. & WHITE, E. S. 2012. Acellular normal and fibrotic human lung matrices as a culture system for in vitro investigation. *Am J Respir Crit Care Med,* 186**,** 866-76.

CEREIJIDO, M., ROBBINS, E. S., DOLAN, W. J., ROTUNNO, C. A. & SABATINI, D. D. 1978. Polarized Monolayers Formed by Epithelial-Cells on a Permeable and Translucent Support. *Journal of Cell Biology,* 77**,** 853-880.

DALTON, P. D., VAQUETTE, C., FARRUGIA, B. L., DARGAVILLE, T. R., BROWN, T. D. & HUTMACHER, D. W. 2012. Electrospinning and additive manufacturing: converging technologies. *Biomater. Sci.,* 1**,** 171-185.

DIXON, J. E., DICK, E., RAJAMOHAN, D., SHAKESHEFF, K. M. & DENNING, C. 2011. Directed differentiation of human embryonic stem cells to interrogate the cardiac gene regulatory network. *Mol Ther,* 19**,** 1695-703.

DIXON, J.E., SHAH, D.A., ROGERS, C., HALL, S., WESTON, N., PARMENTER, C.D., McNALLY, D., DENNING, C. & SHAKESHEFF, K.M. 2014. Combined hydrogelsthat switch human pluipotent stem cells from self-renewal to differentiation. *PNAS*, 111, 5580-5.

DOBRIN, P. B. 1978. Mechanical-Properties of Arteries. *Physiological Reviews,* 58**,** 397-460.

ENGLER, A. J., SEN, S., SWEENEY, H. L. & DISCHER, D. E. 2006. Matrix elasticity directs stem cell lineage specification. *Cell,* 126**,** 677-89.

GUMBINER, B. & SIMONS, K. 1986. A functional assay for proteins involved in establishing an epithelial occluding barrier: identification of a uvomorulin-like polypeptide. *J Cell Biol,* 102**,** 457-68.

GUMBINER, B. M. 1996. Cell adhesion: the molecular basis of tissue architecture and morphogenesis. *Cell,* 84**,** 345-57.

IVANOV, A. I., MCCALL, I. C., PARKOS, C. A. & NUSRAT, A. 2004a. Role for actin filament turnover and a myosin II motor in cytoskeleton-driven disassembly of the epithelial apical junctional complex. *Mol Biol Cell,* 15**,** 2639-51.

IVANOV, A. I., NUSRAT, A. & PARKOS, C. A. 2004b. Endocytosis of epithelial apical junctional proteins by a clathrin-mediated pathway into a unique storage compartment. *Mol Biol Cell,* 15**,** 176-88.

JEFFERY, P. K. 2001. Remodeling in asthma and chronic obstructive lung disease. *Am J Respir Crit Care Med,* 164**,** S28-38.

JUNGEBLUTH, P., ALICI, E., BAIGUERA, S., LE BLANC, K., BLOMBERG, P., BOZOKY, B., CROWLEY, C., EINARSSON, O., GRINNEMO, K. H., GUDBJARTSSON, T., LE GUYADER, S., HENRIKSSON, G., HERMANSON, O., JUTO, J. E., LEIDNER, B., LILJA, T., LISKA, J., LUEDDE, T., LUNDIN, V., MOLL, G., NILSSON, B., RODERBURG, C., STROMBLAD, S., SUTLU, T., TEIXEIRA, A. I., WATZ, E., SEIFALIAN, A. & MACCHIARINI, P. 2011. Tracheobronchial transplantation with a stem-cell-seeded bioartificial nanocomposite: a proof-of-concept study. *Lancet,* 378**,** 1997-2004.

KAKISIS, J. D., LIAPIS, C. D., BREUER, C. & SUMPIO, B. E. 2005. Artificial blood vessel: the Holy Grail of peripheral vascular surgery. *J Vasc Surg,* 41**,** 349-54.

KARAMAN, B., BATTAL, B., BOZKURT, Y., BOZLAR, U., DEMIRKOL, S., SAHIN, M. A. & TASAR, M. 2012. The anatomic evaluation of the internal mammary artery using multidetector CT angiography. *Diagn Interv Radiol,* 18**,** 215-20.

KAUR, D., SAUNDERS, R., BERGER, P., SIDDIQUI, S., WOODMAN, L., WARDLAW, A., BRADDING, P. & BRIGHTLING, C. E. 2006. Airway smooth muscle and mast cell-derived CC chemokine ligand 19 mediate airway smooth muscle migration in asthma. *Am J Respir Crit Care Med,* 174**,** 1179-88.

KHEIRABADI, B. S., SIEBER, J. & HOLCOMB, J. B. 2006. Assessment of the thrombogenic effect of fibrin sealant dressing in a vascular surgery model in rabbits. *J Invest Surg*, 19(6), 387-96.

KIM, M. J., KIM, J. H., YI, G., LIM, S. H., HONG, Y. S. & CHUNG, D. J. 2008. In vitro and in vivo application of PLGA nanofiber for artificial blood vessel. *Macromolecular Research,* 16**,** 345-352.

KUBO, H., SHIMIZU, T., YAMATO, M., FUJIMOTO, T. & OKANO, T. 2007. Creation of myocardial tubes using cardiomyocyte sheets and an in vitro cell sheet-wrapping device. *Biomaterials,* 28**,** 3508-16.

KWAK, Y. K., VIKSTROM, E., MAGNUSSON, K. E., VECSEY-SEMJEN, B., COLQUE-NAVARRO, P. & MOLLBY, R. 2012. The Staphylococcus aureus alpha-toxin perturbs the barrier function in Caco-2 epithelial cell monolayers by altering junctional integrity. *Infect Immun,* 80**,** 1670-80.

L'HEUREUX, N., DUSSERRE, N., KONIG, G., VICTOR, B., KEIRE, P., WIGHT, T. N., CHRONOS, N. A., KYLES, A. E., GREGORY, C. R., HOYT, G., ROBBINS, R. C. & MCALLISTER, T. N. 2006. Human tissue-engineered blood vessels for adult arterial revascularization. *Nat Med,* 12**,** 361-5.

L'HEUREUX, N., PAQUET, S., LABBE, R., GERMAIN, L. & AUGER, F. A. 1998. A completely biological tissue-engineered human blood vessel. *FASEB J,* 12**,** 47-56.

MCALLISTER, T. N. & L'HEUREUX, N. 2006. Bioreactor for the manufacture of tissue engineered blood vessels. US Patent 7744526 B2.

MCALLISTER, T. N., MARUSZEWSKI, M., GARRIDO, S. A., WYSTRYCHOWSKI, W., DUSSERRE, N., MARINI, A., ZAGALSKI, K., FIORILLO, A., AVILA, H., MANGLANO, X., ANTONELLI, J., KOCHER, A., ZEMBALA, M., CIERPKA, L., DE LA FUENTE, L. M. & L'HEUREUX, N. 2009. Effectiveness of haemodialysis access with an autologous tissue-engineered vascular graft: a multicentre cohort study. *Lancet,* 373**,** 1440-6.

MORRIS, G. E., BRIDGE, J. C., ELTBOLI, O. M., KNOX, A. J., AYLOTT, J. W., BRIGHTLING, C. E., GHAEMMAGHAMI, A. M. & ROSE, F. R. 2014. Human airway smooth muscle maintain in situ orientation and phenotype when cultured on aligned electrospun scaffolds. Am J Physiol Lung Cell Mol Physiol. 307(1). L38-47.

MULLIN, J. M., AGOSTINO, N., RENDON-HUERTA, E. & THORNTON, J. J. 2005. Epithelial and endothelial barriers in human disease. *Drug Discovery Today,* 10**,** 395-408.

NEREM, R. M. & SELIKTAR, D. 2001. Vascular tissue engineering. *Annu Rev Biomed Eng,* 3**,** 225-43.

NIKLASON, L. E., GAO, J., ABBOTT, W. M., HIRSCHI, K. K., HOUSER, S., MARINI, R. & LANGER, R. 1999. Functional arteries grown in vitro. *Science,* 284**,** 489-93.

PAIK, I., SCURR, D. J., MORRIS, B., HALL, G., DENNING, C., ALEXANDER, M. R., SHAKESHEFF, K. M. & DIXON, J. E. 2012. Rapid micropatterning of cell lines and human pluripotent stem cells on elastomeric membranes. *Biotechnol Bioeng,* 109**,** 2630-41.

PAPENBURG, B. J., LIU, J., HIGUERA, G. A., BARRADAS, A. M., DE BOER, J., VAN BLITTERSWIJK, C. A., WESSLING, M. & STAMATIALIS, D. 2009. Development and analysis of multi-layer scaffolds for tissue engineering. *Biomaterials,* 30**,** 6228-39.

PATTERSON, J. T., GILLILAND, T., MAXFIELD, M. W., CHURCH, S., NAITO, Y., SHINOKA, T. & BREUER, C. K. 2012. Tissue-engineered vascular grafts for use in the treatment of congenital heart disease: from the bench to the clinic and back again. *Regen Med,* 7**,** 409-19.

PECK, M., GEBHART, D., DUSSERRE, N., MCALLISTER, T. N. & L'HEUREUX, N. 2012. The evolution of vascular tissue engineering and current state of the art. *Cells Tissues Organs,* 195**,** 144-58.

RHODIN, R. A. J. 1980. Architecture of the Vessel Wall. *Handbook of Physiology, The Cardiovascular System, Vascular Smooth Muscle***,** 1-31.

SCHNEEBERGER, E. E. & LYNCH, R. D. 2004. The tight junction: a multifunctional complex. *Am J Physiol Cell Physiol,* 286**,** C1213-28.

SELIKTAR, D., BLACK, R. A., VITO, R. P. & NEREM, R. M. 2000. Dynamic mechanical conditioning of collagen-gel blood vessel constructs induces remodeling in vitro. *Ann Biomed Eng,* 28**,** 351-62.

SHIMIZU, T., SEKINE, H., YANG, J., ISOI, Y., YAMATO, M., KIKUCHI, A., KOBAYASHI, E. & OKANO, T. 2006. Polysurgery of cell sheet grafts overcomes diffusion limits to produce thick, vascularized myocardial tissues. *FASEB J,* 20**,** 708-10.

SHIMIZU, T., YAMATO, M., KIKUCHI, A. & OKANO, T. 2001. Two-dimensional manipulation of cardiac myocyte sheets utilizing temperature-responsive culture dishes augments the pulsatile amplitude. *Tissue Eng,* 7**,** 141-51.

SHIN'OKA, T., IMAI, Y. & IKADA, Y. 2001. Transplantation of a tissue-engineered pulmonary artery. *N Engl J Med,* 344**,** 532-3.

SHIN'OKA, T., MATSUMURA, G., HIBINO, N., NAITO, Y., WATANABE, M., KONUMA, T., SAKAMOTO, T., NAGATSU, M. & KUROSAWA, H. 2005. Midterm clinical result of tissue-engineered vascular autografts seeded with autologous bone marrow cells. *J Thorac Cardiovasc Surg,* 129**,** 1330-8.

SHUM-TIM, D., STOCK, U., HRKACH, J., SHINOKA, T., LIEN, J., MOSES, M. A., STAMP, A., TAYLOR, G., MORAN, A. M., LANDIS, W., LANGER, R., VACANTI, J. P. & MAYER, J. E., JR. 1999. Tissue engineering of autologous aorta using a new biodegradable polymer. *Ann Thorac Surg,* 68**,** 2298-304; discussion 2305.

TEO, W. E. & RAMAKRISHNA, S. 2006. A review on electrospinning design and nanofibre assemblies. *Nanotechnology,* 17**,** R89-R106.

VAN ANDEL, C. J., PISTECKY, P. V. & BORST, C. 2003. Mechanical properties of porcine and human arteries: implications for coronary anastomotic connectors. *Ann Thorac Surg,* 76**,** 58-64; discussion 64-5.

WANG, S., MO, X. M., JIANG, B. J., GAO, C. J., WANG, H. S., ZHUANG, Y. G. & QIU, L. J. 2013. Fabrication of small-diameter vascular scaffolds by heparin-bonded P(LLA-CL) composite nanofibers to improve graft patency. *Int J Nanomedicine,* 8**,** 2131-9.

WILLIAMS, C., TSUDA, Y., ISENBERG, B. C., YAMATO, M., SHIMIZU, T., OKANO, T. & WONG, J. Y. 2009. Aligned Cell Sheets Grown on Thermo-Responsive Substrates with Microcontact Printed Protein Patterns. *Advanced Materials,* 21**,** 2161-+.

WILLIAMS, C., XIE, A. W., YAMATO, M., OKANO, T. & WONG, J. Y. 2011. Stacking of aligned cell sheets for layer-by-layer control of complex tissue structure. *Biomaterials,* 32**,** 5625-32.

YE, J., TSUKAMOTO, T., SUN, A. & NIGAM, S. K. 1999. A role for intracellular calcium in tight junction reassembly after ATP depletion-repletion. *Am J Physiol,* 277**,** F524-32.

YUAN, B., JIN, Y., SUN, Y., WANG, D., SUN, J., WANG, Z., ZHANG, W. & JIANG, X. 2012. A strategy for depositing different types of cells in three dimensions to mimic tubular structures in tissues. *Adv Mater,* 24**,** 890-6.

Figure 1.

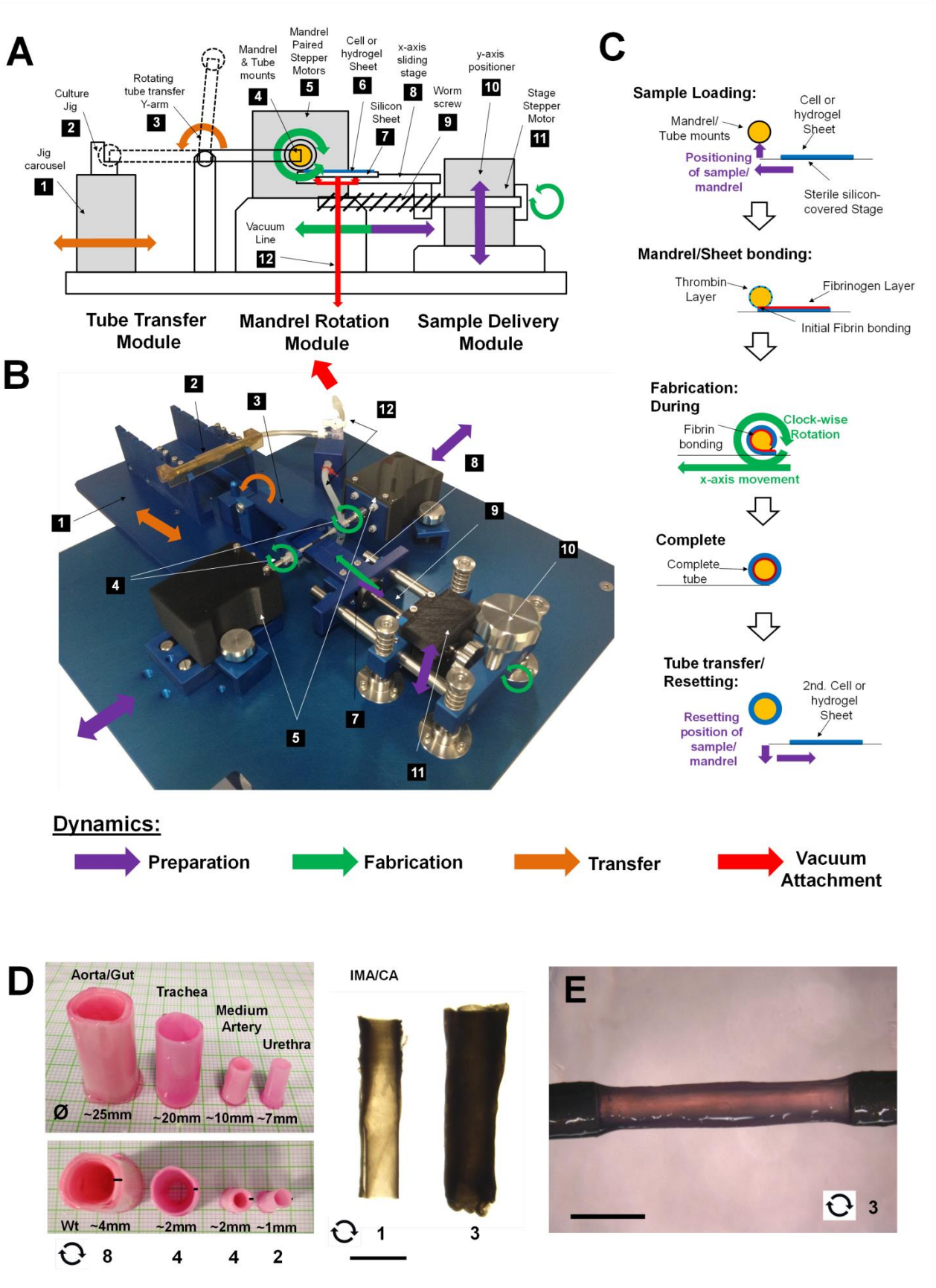
A
Culture Jig
2
Rotating tube transfer Y-arm
3
Mandrel & Tube mounts
4
Mandrel Paired Stepper Motors
5
Cell or hydrogel Sheet
6
x-axis sliding stage
8
Worm screw
9
y-axis positioner
10
Stage Stepper Motor
11
Silicon Sheet
7
Jig carousel
1
Vacuum Line
12
Tube Transfer Module
Mandrel Rotation Module
Sample Delivery Module
B
C
Sample Loading:
Mandrel/ Tube mounts
Cell or hydrogel Sheet
Positioning of sample/ mandrel
Sterile silicon-covered Stage
Mandrel/Sheet bonding:
Thrombin Layer
Fibrinogen Layer
Initial Fibrin bonding
Fabrication: During
Fibrin bonding
Clock-wise Rotation
x-axis movement
Complete
Complete tube
Tube transfer/ Resetting:
Resetting position of sample/ mandrel
2nd. Cell or hydrogel Sheet
Dynamics:
Preparation
Fabrication
Transfer
Vacuum Attachment
D
Aorta/Gut
Trachea
Medium Artery
Urethra
Ø ~25mm
~20mm
~10mm
~7mm
Wt ~4mm
~2mm
~2mm
~1mm
8
4
4
2
IMA/CA
1
3
E
3

Figure 1. Automated tube fabricator (ATF) and fabricated vessels. **A)** Schematic of ATF. Sample sheets are delivered through an x-axis sliding stage from a computerised stepper motor (which can be positioned in the y-axis; purple). Tubes are rolled onto a mandrel driven by paired computerised stepper motors (green). Samples are attached to the stage using a vacuum line (red). After rolling, the machine may be reset to roll subsequent layers or the tube transferred to culture jigs (orange). **B)** Photograph of the ATF. Numbers indicate the features as described on the schematic. **C)** Flow diagram of tube fabrication process including the movements of the ATF (colour labels match the scheme and photograph). **D)** Examples of tubular constructs of different sizes and thicknesses fabricated using the ATF. Tubes were fabricated from PET electrospun scaffolds and alginate. These mimic the gross dimensions of Aorta/gut, Trachea, Medium artery and Urethra (left-right). Top image shows tube diameter bottom image shows wall thickness (wt). Rotation symbol indicates the number of rotations/layers used for fabrication. Examples of two internal mammary artery (IMA)/ coronary artery (CA) sized vessels with 1 or 3 rotations. **E)** Example of a vessel fabricated by the ATF (with IMA dimensions) within the perfusion bioreactor system. Bar is 3mm.

Figure 2.

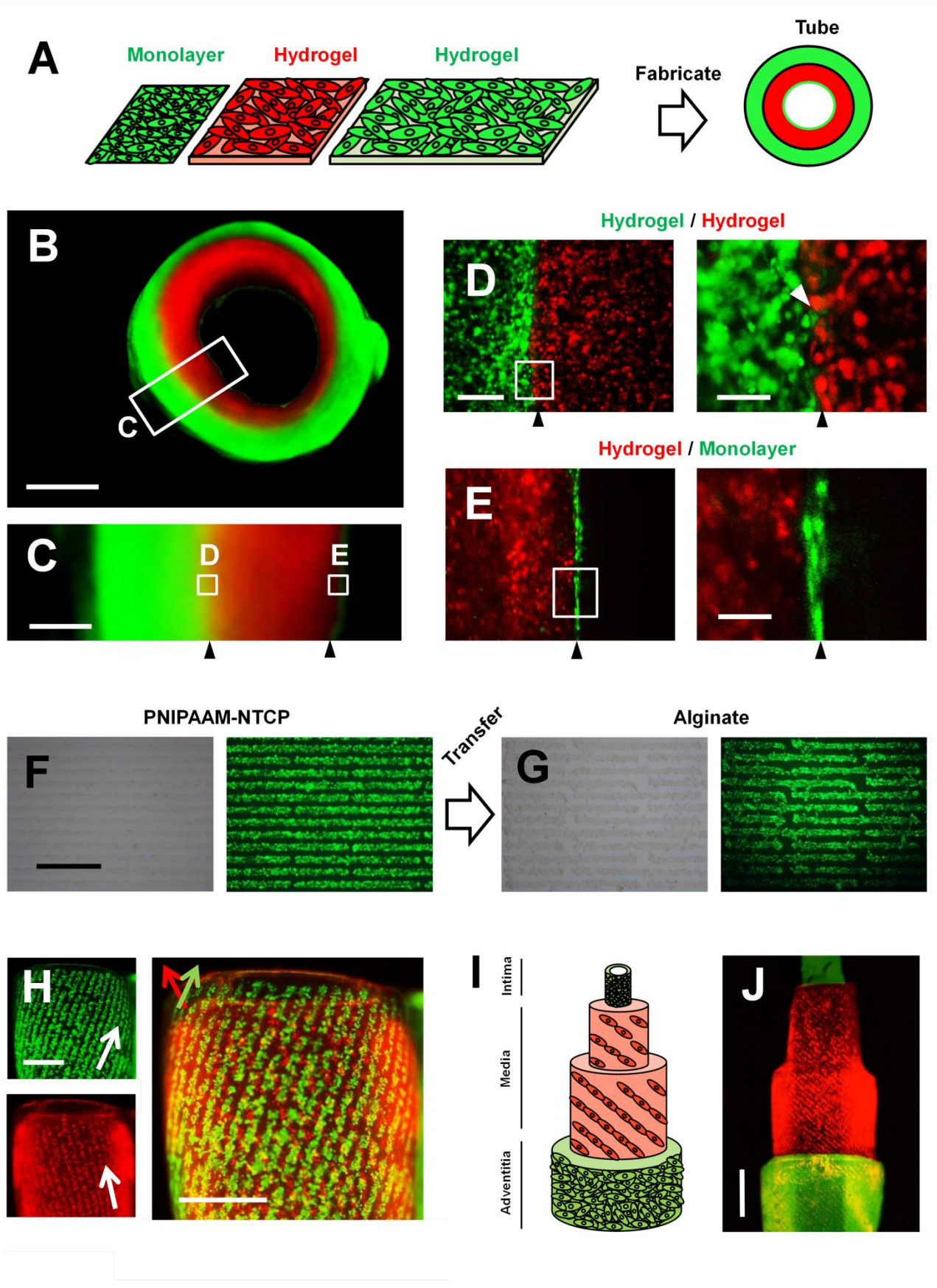
A
Monolayer
Hydrogel
Hydrogel
Fabricate
Tube
B
C
D
E
Hydrogel / Hydrogel
Hydrogel / Monolayer
PNIPAAM-NTCP
Transfer
Alginate
F
G
H
I
Intima
Media
Adventitia
J

Figure 2. Multi-layer & -thickness vessel fabrication. **A)** Schematic of the monolayer and collagen hydrogel sheets employed for multi-layer and –thickness tube fabrication using fluorescently labelled NIH3t3 cells. **B)** Cross-sectional image of the multiple layers within fabricated tube. Bar is 2 mm. **C)** High-magnification images of the interface between the hydrogels (D) and the monolayer/hydrogel (E) layers within tube wall. Black arrows show phase interface. Bar is 2mm. **D)** Confocal image showing complete integration of both hydrogel layers and interaction of cells from both layers. **E)** Confocal image showing interaction of cell monolayer and hydrogel layer. Bar is 100µm on left panel and 20µm on right panel in D & E. Black bars show phase interface. **F)** Representative 2D cell-sheet patterning (50µm width with 50µm gaps). Patterned PNIPAAm-polystyrene surfaces with GFP-labelled NIH3t3s cells (Bright-field and fluorescence images). Bar is 200µm. **G)** Transfer of patterned cells to alginate hydrogel sheet (Bright-field and fluorescence images). **H)** Alginate sheets patterned with GFP- and mRFP labelled NIH3t3 cells were excised to produce angled (horizontal +/- 30˚; 60 and 120˚) 2D cell-sheets and rolled on the AFM to produce a tubular herringbone pattern; green-only, red-only and merged channels are shown. Bar is 1.5mm. **I)** Schematic of a muscular artery structure (0.3-10mm diameter vessels) showing Intima (Endothelial), Media (Smooth muscle) and Adventitia (Fibroblast). **J)** Fabrication of Biomimetic vessels. Fluorescently-labelled human endothelial (HUVEC-GFP), smooth muscle cells (SMC-mRFP) and fibroblasts (BJ6-GFP) were sequentially rolled to fabricate a tube mimicking muscular vessel architecture. The vessel was fabricated to create a sectioned structure to aid visualization. Bar is 2mm.

Figure 3.

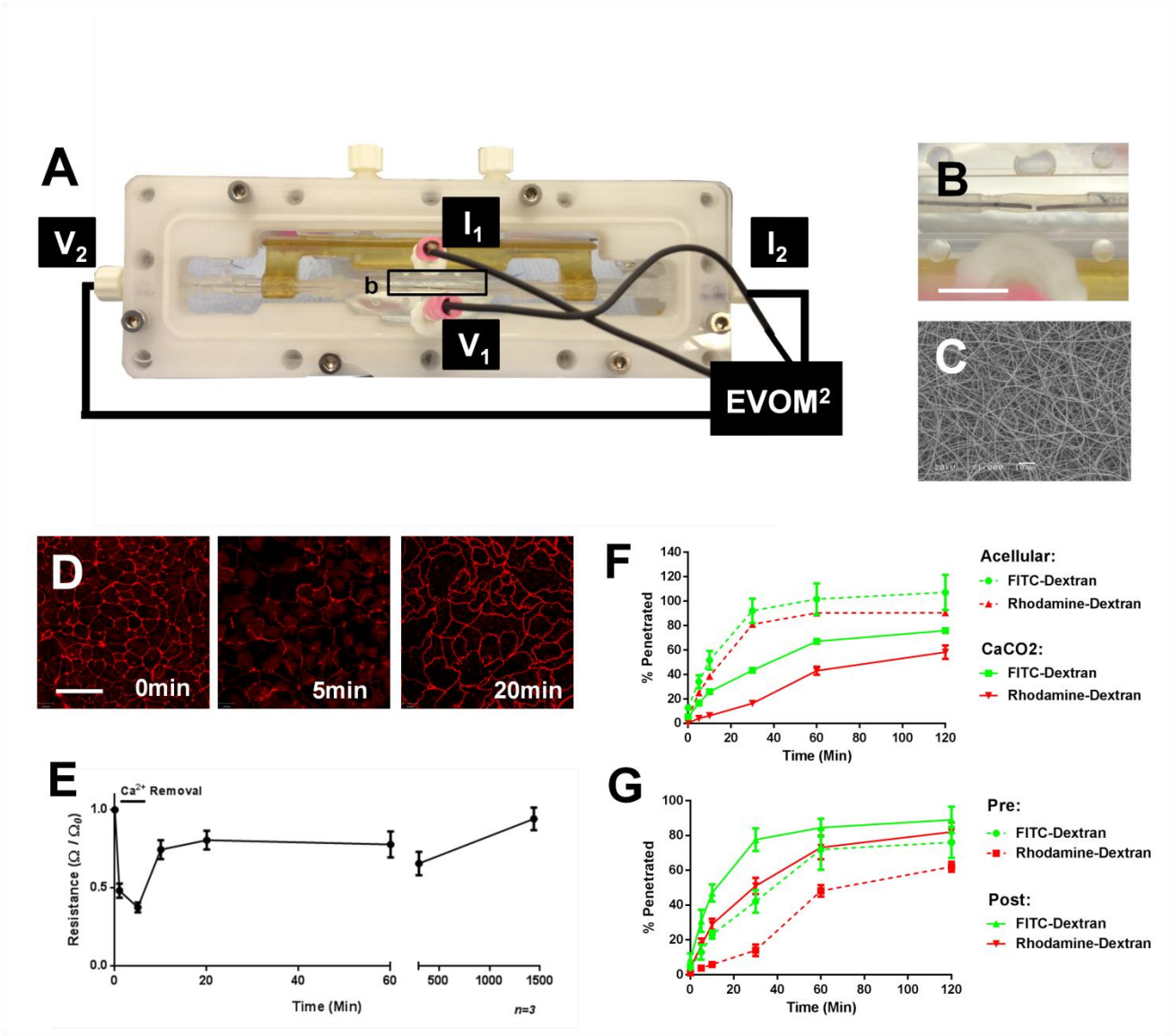
A
V2
I1
I2
b
V1
EVOM2
B
C
D
0min
5min
20min
E
Ca2+ Removal
Resistance (Ω / Ω0)
Time (Min)
n=3
F
% Penetrated
Time (Min)
Acellular:
FITC-Dextran
Rhodamine-Dextran
CaCO2:
FITC-Dextran
Rhodamine-Dextran
G
% Penetrated
Time (Min)
Pre:
FITC-Dextran
Rhodamine-Dextran
Post:
FITC-Dextran
Rhodamine-Dextran

Figure 3. Real-time measurements of vessels. **A)** Photograph of perfusion bioreactor containing a tubular construct. The construct is held in position on culture jigs and is continually perfused using a peristaltic pump. Tube is shown with electrodes connected to an EVOM^2 machine to allowing measurements of real-time electrical resistance (TEER); Amplitude (I) and voltage (V) are measured within the lumen (V2 & I2) and externally to the tube within the perfusion chamber (I1 & V1). **B)** Photograph of construct secured in perfusion chamber with electrodes inserted within lumen. Bar is 10mm. **C)** Scanning electron microscope image of an acellular PET electrospun scaffold. Bar is 10µm. **D)** Immunostaining of E-Cadherin (red) in a confluent layer of CACO-2 cells on the PET electrospun scaffold before Ca^{2+} depletion, 5min, and 20min post-Ca^{2+} depletion (left to right). Bar is 60µm. **E)** Electrical resistance through CACO-2 tube after Ca^{2+} depletion. CACO-2-populated PET electrospun scaffold tube was fabricated and loaded into the perfusion bioreactor with electrodes placed as shown in (A). Ca^{2+} was depleted for 5min before replacement in normal media. Electrical resistance was measured periodically over a 24hr period. **F)** Para-cellular permeability through a CACO-2 tube. Acellular and CACO-2 populated electrospun tubes were placed in perfusion bioreactor. Serum-free media containing both 4kDa FITC-tagged and 70kDa Rhodamine-tagged dextran was perfused through the tube lumen. Samples from the perfusion chamber were taken over a 2hr period, and fluorescence expressed as a percentage of total initial fluorescence. **G)** Para-cellular permeability through a CACO-2 tube pre- and post-Ca^{2+} depletion.

Figure S1.

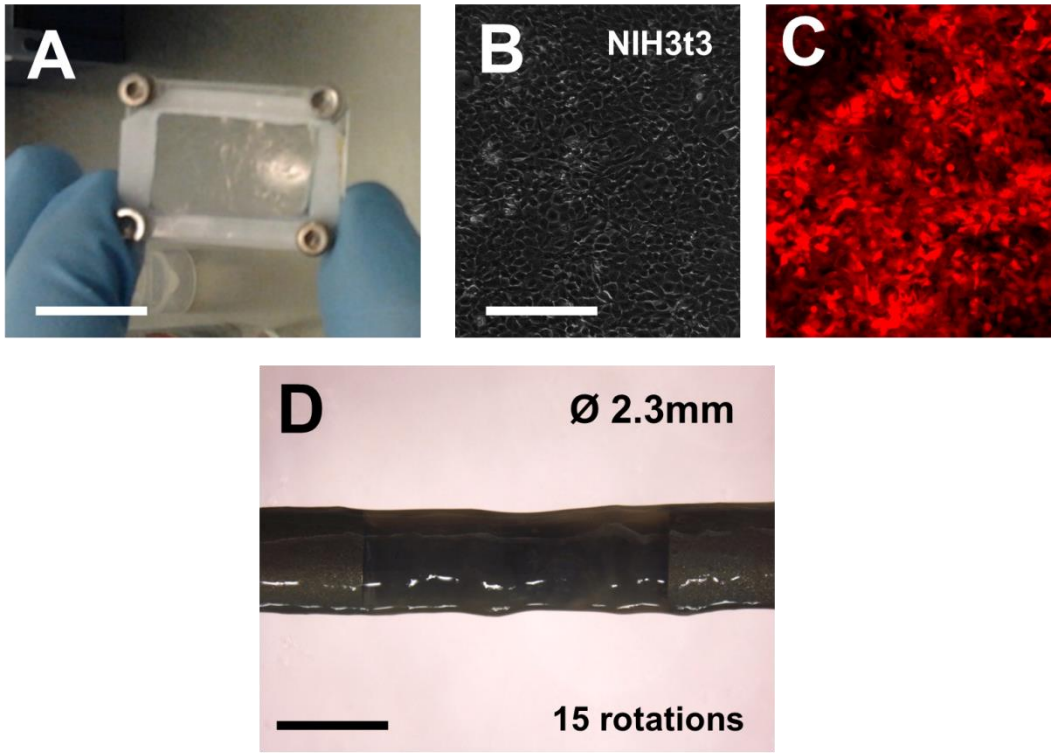

Figure S1. Detachment of cell-only sheets and vessel fabrication. **A)** A mRFP-labelled NIH3t3 monolayer cell-only sheet detached from a PNIPAAm surface by lowering temperature. Sheets were transferred on filter paper frames (coated in cross-linked alginate). Bar is 12mm. **B)** Light and **C)** fluorescence microscopy of a detached mRFP-labelled NIH3t3 sheet. Bar is 100µm. A tube fabricated using the ATF from a cell-only sheet with 3 (Figure 1E) or **D)** 15 rotations. Bar is 3mm. Ø is tube diameter.

Figure S2.

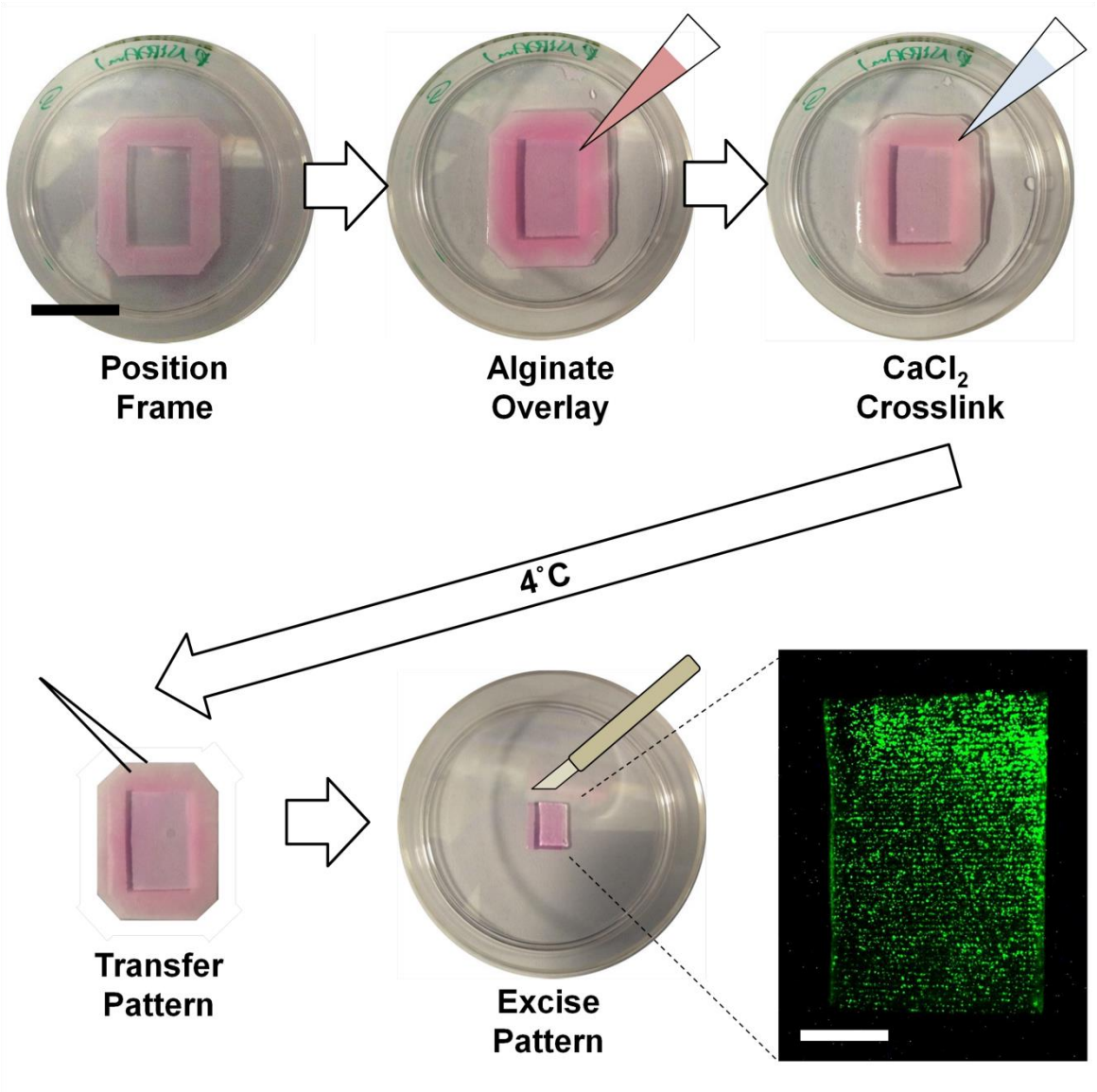

Figure S2. Cell pattern transfer for tube fabrication. A flow diagram using photographic images of the process used to pattern cells on PNIPAAM-coated polystyrene and subsequently transfer patterns to alginate sheets. Bar is 20mm.

Figure S3.

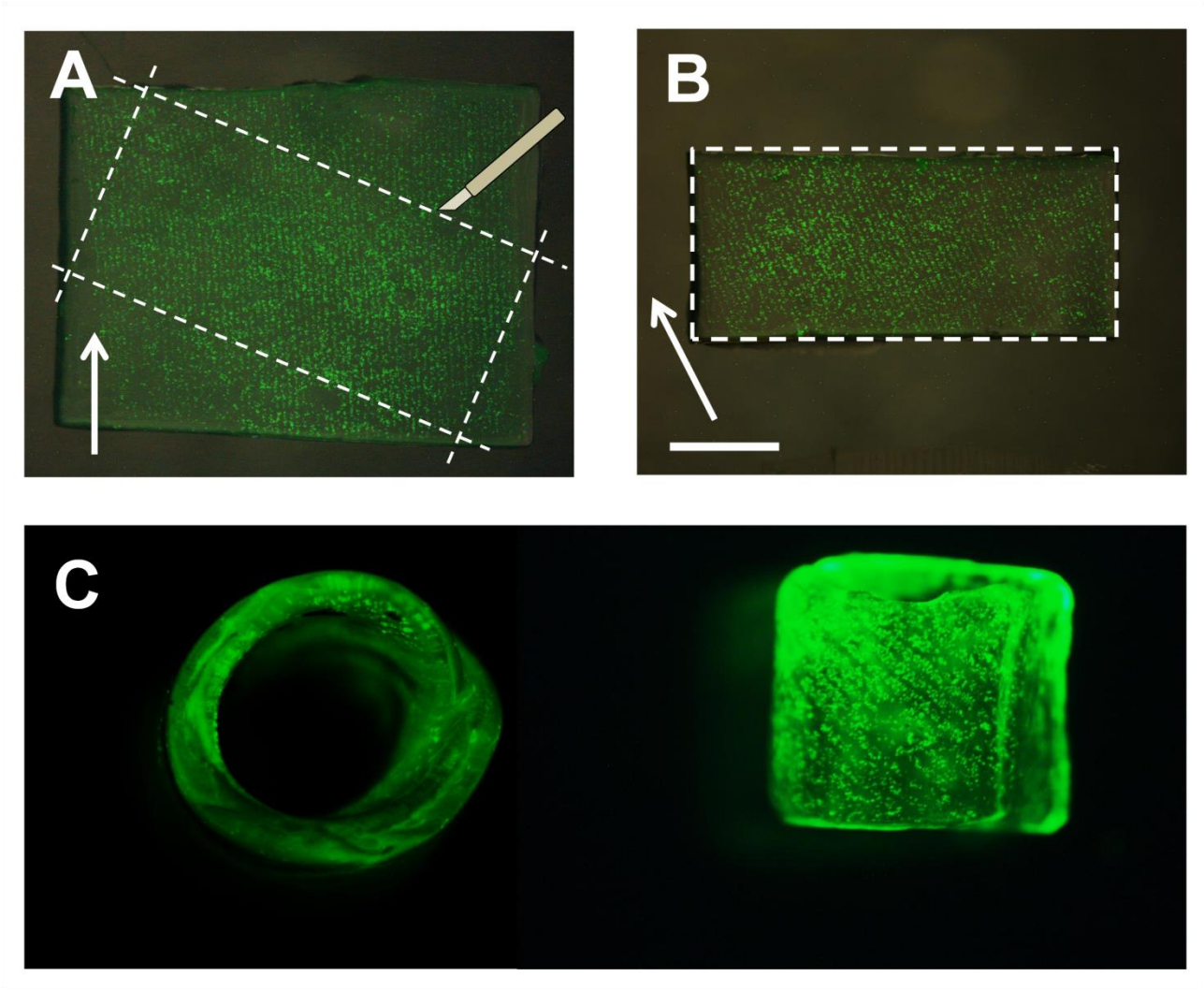

Figure S3. Excision of cell patterns for tube fabrication. **A)** A GFP-labelled NIH3t3 hydrogel sheet was excised to produce sheets of required cell orientations. **B)** An excised sheet with cell lines 60˚ from horizontal. **C)** A tube fabricated using the ATF from the sheet in B) showing helically orientated cells patterns. Bar is 0.5mm.